Supplementary Materials

Recyclable TiO_2–Fe_3O_4 Magnetic Composites for the Photocatalytic Degradation of Paracetamol: Effect of TiO_2 Phase Composition

Kata Saszet [1,2], Simona Guliman [3], Lilla Szalma [4], István Székely [1,2], Romulus Tetean [1], Milica Todea [5,6], Ákos Szamosvölgyi [4], Marieta Mureșan-Pop [2,6], Lucian Barbu-Tudoran [7,8], Klára Magyari [2,9], Lucian-Cristian Pop [3], Zsolt Pap [2,4,10*], Lucian Baia [1,2,10*]

[1] Faculty of Physics, Babeș-Bolyai University, M. Kogălniceanu St. 1, RO-400084 Cluj-Napoca, Romania;
[2] Nanostructured Materials and Bio-Nano-Interfaces Center, Interdisciplinary Research Institute on Bio-Nano-Sciences, Babeș-Bolyai University, Treboniu Laurian St. 42, RO-400271 Cluj-Napoca, Romania;
[3] Faculty of Chemistry and Chemical Engineering, Babeș-Bolyai University, Arany János St. 11, RO-400028 Cluj-Napoca, Romania;
[4] Department of Applied and Environmental Chemistry, University of Szeged, Rerrich Béla Sqr. 1, H-6720 Szeged, Hungary;
[5] Department of Molecular Sciences, Faculty of Medicine, Iuliu Haţieganu University of Medicine and Pharmacy, Victor Babeș St. 8, RO-400012 Cluj-Napoca, Romania;
[6] Contrast Agents and Specific Therapeutics Center—INSPIRE Platform, Interdisciplinary Research Institute in Bio-Nano-Sciences, Babeș-Bolyai University, Treboniu Laurian St. 42, RO-400271 Cluj-Napoca, Romania;
[7] Electron Microscopy Center, Faculty of Biology and Geology, Babeș-Bolyai University, Clinicilor St. 5-7, RO-400006 Cluj-Napoca, Romania;
[8] National Institute for Research and Development of Isotopic and Molecular Technologies, Donat St. 67-103, RO-400293 Cluj-Napoca, Romania;
[9] INSPIRE Research Platform InfoBioNano4Health & Biomedical Imaging, Babeș-Bolyai University, Arany János St. 11, RO-400084 Cluj-Napoca, Romania;
[10] Laboratory for Advanced Materials and Applied Technologies, Institute of Research-Development-Innovation in Applied Natural Sciences, Babes-Bolyai University, Fântânele St. 30, RO-400327 Cluj-Napoca, Romania;

Results and discussion – Supplementary Results

S2.1. Structural and morphological characterization of IONPs.

With the objective of choosing an iron oxide nanoparticle (IONP) with suitable properties for magnetic composite preparation, four IONP samples were synthesized under different experimental conditions. These conditions involved varying the preparation temperature and concentration of the applied NaOH solution, as detailed in Table S1, which also presents the corresponding sample names based on their synthesis parameters.

Table S1. Overview of properties of IONPs synthesized in various conditions.

Sample name	NaOH concentration [M]	Synthesis temperature [°C]	Primary crystallite size [nm]	Crystallinity degree [%]
IONP_0.4_25	0.4	25	33.3	68.23%
IONP_0.4_75	0.4	75	43.7	71.47%
IONP_0.8_25	0.8	25	23.2	87.98%
IONP_0.8_75	0.8	75	46.4	76.45%

The selection was preceded by a series of structural and morphological characterizations of the IONPs.

First of all, to learn about the success of the synthesis, the crystal phase composition and crystal structure of the samples had to be investigated. Hence, the XRD patterns of the four IONPs were recorded and presented in Figure S1. All four samples displayed the same reflections on their diffractogram, with occasional shifts of less than 0.1 (2θ)° from each other: thirteen reflections attributed to the cubic crystal phase of magnetite (Fe_3O_4 - JCPDS card no. 19-0629). The reflections identified as belonging to Fe_3O_4 in case of IONP_0.4_75 were observed at 2θ: 18.44°, 30.30°, 35.62°, 37.30°, 43.32°, 53.74°, 57.26°, 62.90°, 65.98°, 71.32°, 74.28°, 75.40° and 79.40° and can be attributed to the crystallographic planes (111), (220), (311), (222), (400), (422), (511), (440), (531), (620), (533), (622) and (444), respectively, of cubic Fe_3O_4 [49,62].

Since the control of iron oxide nanoparticle synthesis is challenging, another possible reaction product of this synthesis method could be maghemite (γ-Fe_2O_3 - JCPDS card no. 39-1346). Maghemite from magnetite is typically differentiated in diffractometry through two characteristic reflections at 23.77° and 26.10° with very weak intensity corresponding to planes (210) and (211); and through the position of the reflection attributed to the crystallographic plane (511) [63]. In the present study, the planes (210) and (211) were not observable within the limit of experimental errors. The reflection attributed to the crystallographic plane (511) is located at 57.26°, showing the predominant presence of the magnetite phase (Figure S1).

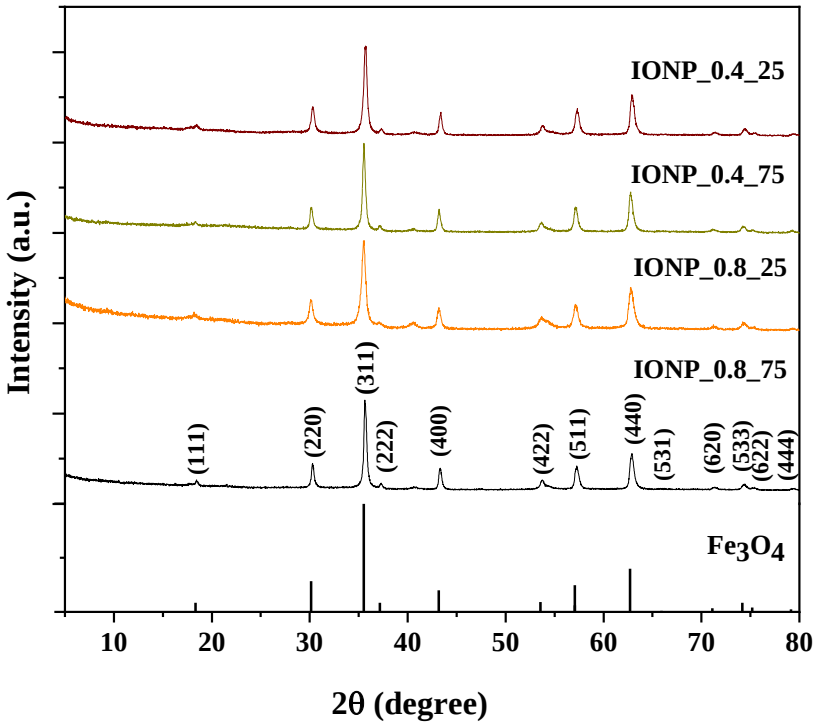


Figure S1. XRD patterns of IONPs synthesized using various NaOH concentrations and temperatures.

The XRD measurements also provided information about the primary crystallite size and the crystallinity degrees of the samples, both characteristics having important roles in the applicability of the IONP. Comparing the primary crystallite size of the samples (Table S1), it can be observed that a higher synthesis temperature allows the formation of larger nanoparticles. The concentration of the used NaOH solution cannot be considered a parameter that unequivocally influences the primary crystallite size. However, a correlation is observable with the crystallinity degree of the IONPs: employing a NaOH solution with higher concentration results in a more crystalline nanomaterial at both 25 ℃ and 75 ℃ (Table S1).

Among the four samples, IONP_0.8_25 exhibits the highest crystallinity but also the smallest primary crystallite size. A more crystalline sample typically corresponds to fewer structural defects, which can indirectly lead to improved magnetic properties. Nonetheless, previous studies have shown that nanoparticles with a smaller mean crystallite size are generally more prone to recrystallization [64]. Therefore, going forward, it already seems preferable to choose IONP_0.8_75, the IONP with the largest crystallite size and second-highest crystallinity degree for incorporation in composites, as it promises greater structural stability besides favorable magnetic properties.

To verify the possible presence of maghemite that stems from the diffractograms, the phase composition of the four IONPs was further investigated. Given that the synthesis of magnetite can result in various by-

products, as mentioned earlier, this is a good opportunity to exclude any other iron oxide or oxide-hydroxide from the composition. For this purpose, Raman spectroscopy measurements were carried out on the four samples. The characteristics of the recorded spectra validated the presence of both magnetite (Fe_3O_4) and maghemite (γ-Fe_2O_3) (Figure S2). The intense characteristic vibrational band of magnetite appears around 674 cm^{-1}, together with two other bands around 307 and 548 cm^{-1}. The bands of maghemite are distinguishable around 714 cm^{-1}, as a shoulder of the previously mentioned magnetite peak, and around 370 cm^{-1} as a broader band [65,66]. Based on the Raman spectra, the vibrational bands of magnetite are the most dominant in sample IONP_0.8_75. The other extreme of the magnetite-maghemite ratio variation is the sample IONP_0.8_25, in which the features of maghemite vibrational modes are the most prominent among the IONPs. Besides magnetite and maghemite, no other components were observable from the Raman spectra.

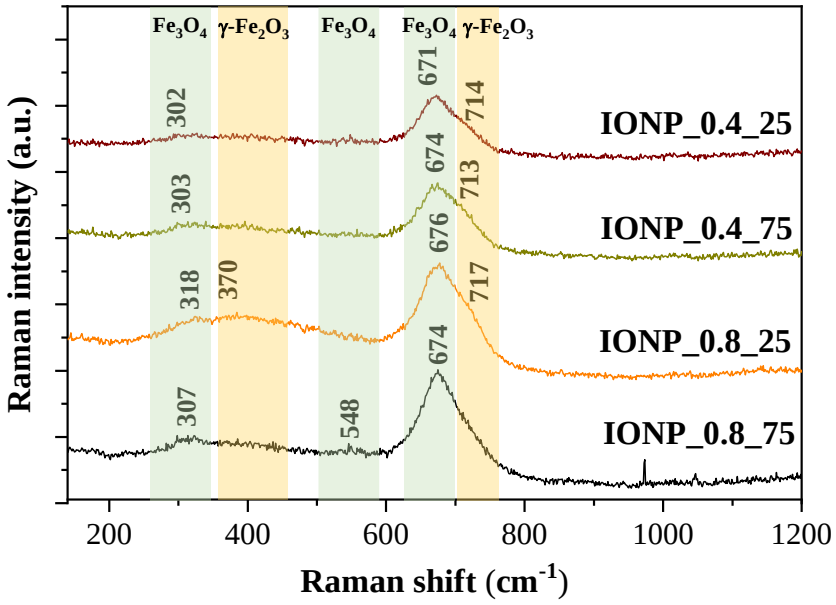


Figure S2. Raman spectra of the IONP samples.

Diffuse reflectance spectra of the IONP samples were also measured to investigate their optical properties; however, the low reflectance values (<10%) limited the reliable estimation of their band gap (Figure S3).

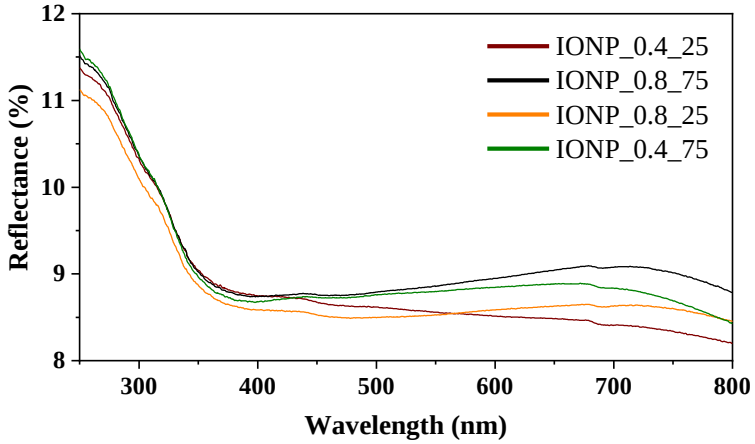


Figure S3. UV-Vis reflectance spectra of IONP samples.

As a last addition to the assessment of material properties, the samples' morphology was investigated *via* SEM (Figure S4). One of the objectives was to determine if the particles exhibited any specific morphology or hierarchical crystal structure, which, considering the lack of a shape-tailoring agent and the precipitation synthesis method, was not expected. The micrographs corroborated this assumption: all samples are polycrystalline and do not take any special, uniform shape. The polygonal grains are organized in aggregates in the case of each sample, with various levels of aggregation from 10 to 100 μm, but a pattern that can be correlated with the variations in the synthesis conditions was not observed. The aggregation of the particles on their own cannot be correlated with the applicability of the IONPs in suspensions, such as in the case of heterogeneous photocatalysis, due to the different mediums. In regard to applicability and choice of suitable IONP for the composite, the findings of the SEM investigations were of no consequence.

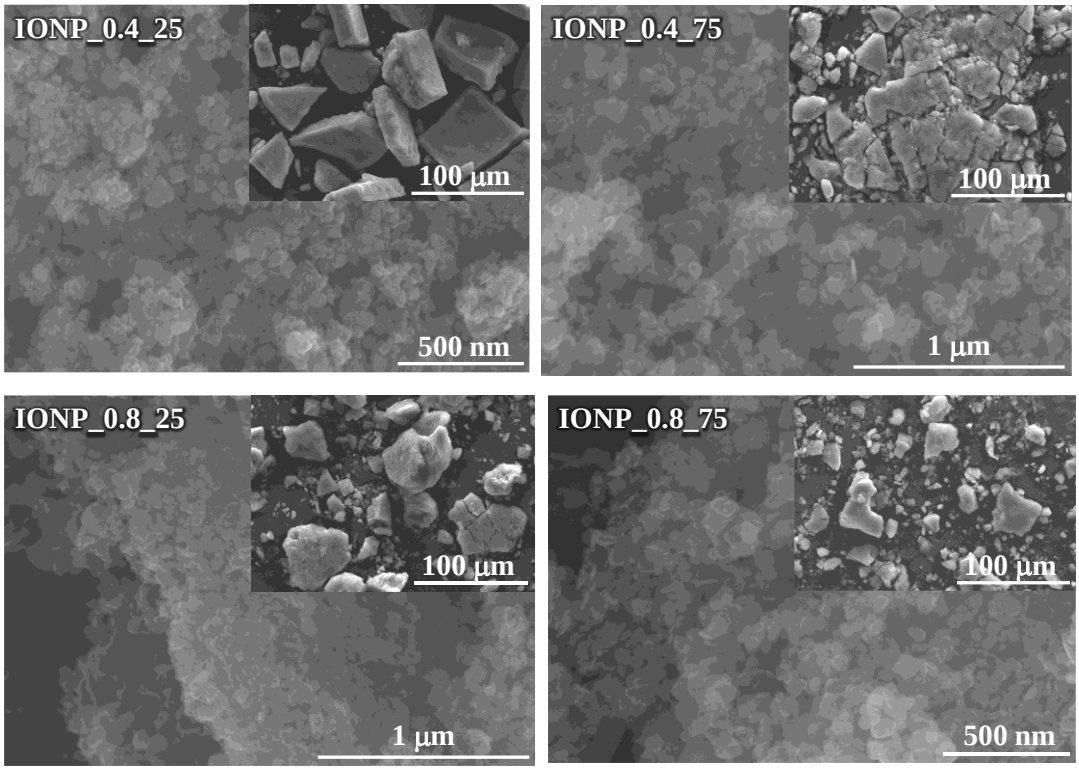


Figure S4. SEM images of iron oxide nanoparticles prepared under various experimental conditions: IONP_0.4_25 – NaOH 0.4 M and 25 ℃, IONP_0.4_75 – NaOH 0.4 M and 75 ℃, IONP_0.8_25 – NaOH 0.8 M and 25 ℃, IONP_0.8_75 – NaOH 0.8 M and 75 ℃.

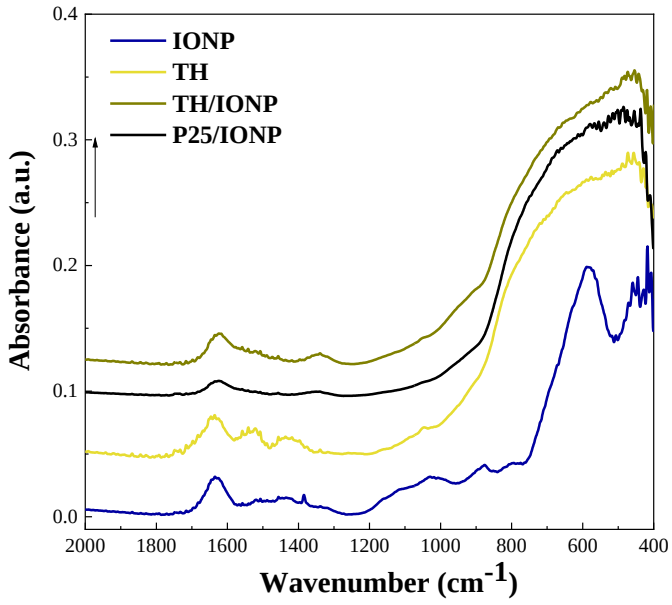


Figure S5. FT-IR spectra of pristine IONP, TiO_2, and their composites.

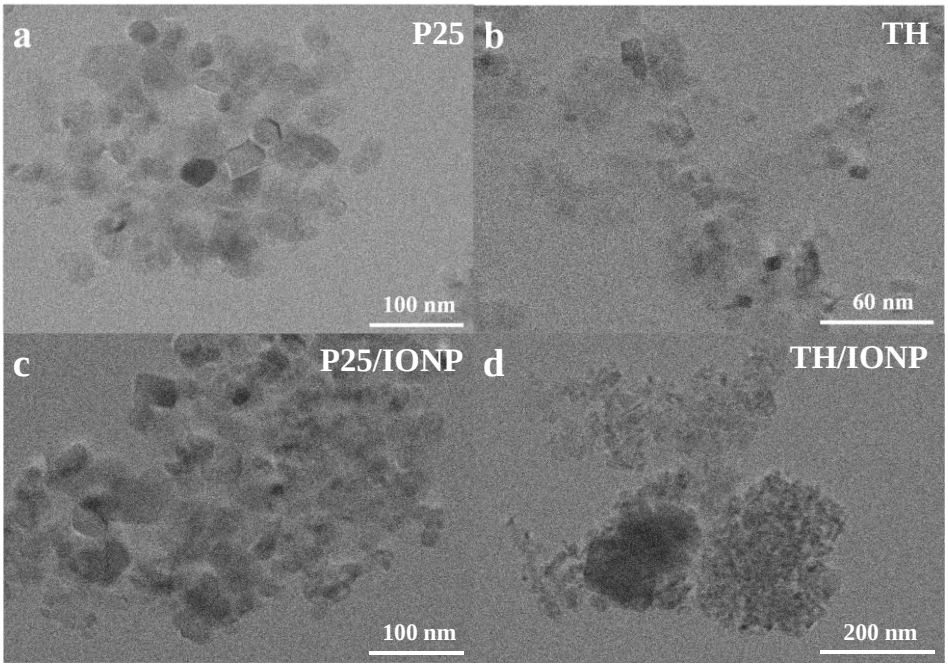


Figure S6. TEM micrographs of pristine TiO_2 TH, P25 and their composites.

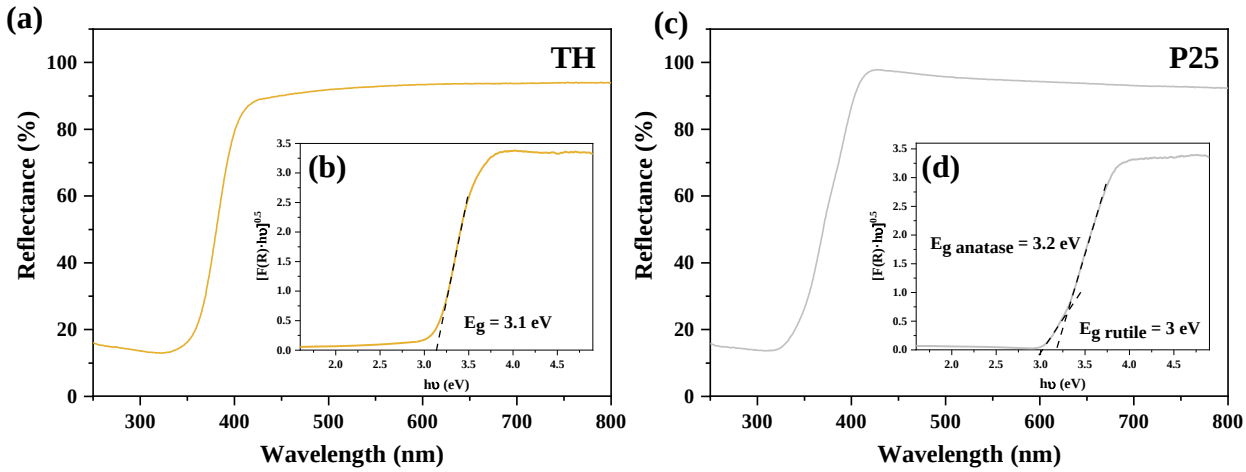


Figure S7. (a) UV-Vis spectra of synthesized TH TiO_2, (b) band gap energy calculation of synthesized TH TiO_2, (c) UV-Vis spectra of P25 TiO_2, (d) band gap energy calculation of P25 TiO_2.

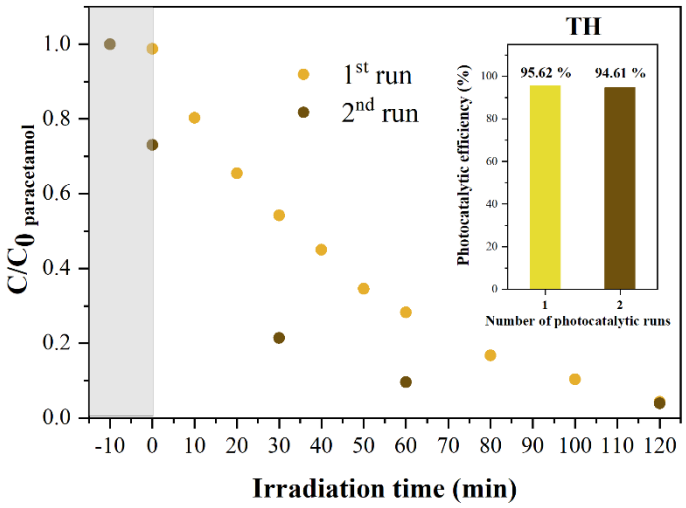


Figure S8. Adsorption properties and photocatalytic activity of the sample TH after the first two photocatalytic runs (repeated experimental set).

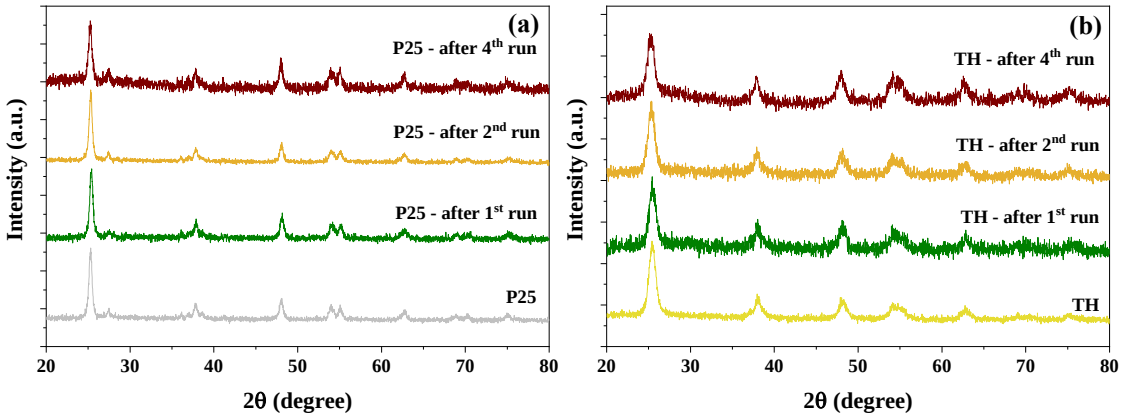


Figure S9. XRD pattern of P25 (a) and TH (b) after synthesis, after 1st, 2nd, and 4th photocatalytic runs.

Table S2. Comparison of the performance of the composite photocatalysts of the present study with the findings of the literature on related catalytic systems

Photocatalyst	Catalyst conc. (g/L)	Pollutant	Pollutant concentration	Degradation efficiency	Degradation time (min)	Recycling rounds	Efficiency after recycling	Ref.
TiO_2- Fe_3O_4	1	Metronidazole	20 mg/L	90%	180	N.A.	N.A.	[29]
Fe_2O_3-TiO_2	1.25	Paracetamol	30 mg/L	98.85%	180	N.A.	N.A.	[67]
Fe_3O_4/TiO_2	0.5	RhB	10 mg/L	91%	120	5	88%	[30]
Fe_3O_4@TiO_2	0.33	Methylene Blue	16 mg/L	97.56%	90	5	89.9%	[57]
TiO_2/Fe_3O_4	2	RhB	5 mg/L	90%	90	4	53.6%	[28]
P25/Fe_3O_4	1	Paracetamol	15.12 mg/L	98.9%	120	4	95.7%	Present study
TiO_2/Fe_3O_4 (TH/IONP)	1	Paracetamol	15.12 mg/L	69.4%	120	4	44.8%	Present study

References of the Supplementary Materials

[28] P. Tang, Y. Ding, H. Chen, Y. Wang, Preparation of TiO_2 /Fe_3O_4 composite by sol-gel method and its photocatalytic activity for removal of Rhodamine B from water, Ferroelectrics 562 (2020) 66–72. https://doi.org/10.1080/00150193.2020.1760594.

[29] A. Kubiak, Comparative study of TiO_2–Fe_3O_4 photocatalysts synthesized by conventional and microwave methods for metronidazole removal, Sci Rep 13 (2023) 12075. https://doi.org/10.1038/s41598-023-39342-9.

[30] N. Madima, K.K. Kefeni, S.B. Mishra, A.K. Mishra, A.T. Kuvarega, Fabrication of magnetic recoverable Fe_3O_4/TiO_2 heterostructure for photocatalytic degradation of rhodamine B dye, Inorg Chem Commun 145 (2022) 109966. https://doi.org/10.1016/j.inoche.2022.109966.

[49] M.E. Compeán-Jasso, F. Ruiz, J.R. Martínez, A. Herrera-Gómez, Magnetic properties of magnetite nanoparticles synthesized by forced hydrolysis, Mater Lett 62 (2008) 4248–4250. https://doi.org/10.1016/j.matlet.2008.06.053.

[57] Q. Zhang, L. Yu, C. Xu, W. Zhang, M. Chen, Q. Xu, G. Diao, A novel method for facile preparation of recoverable Fe_3O_4@TiO_2 core-shell nanospheres and their advanced

photocatalytic application, Chem Phys Lett 761 (2020) 138073. https://doi.org/10.1016/j.cplett.2020.138073.

[62] C. Haavik, S. Stølen, H. Fjellvåg, M. Hanfland, D. Häusermann, Equation of state of magnetite and its high-pressure modification: Thermodynamics of the Fe-O system at high pressure, American Mineralogist 85 (2000) 514–523. https://doi.org/10.2138/am-2000-0413.

[63] W. Kim, C.-Y. Suh, S.-W. Cho, K.-M. Roh, H. Kwon, K. Song, I.-J. Shon, A new method for the identification and quantification of magnetite–maghemite mixture using conventional X-ray diffraction technique, Talanta 94 (2012) 348–352. https://doi.org/10.1016/j.talanta.2012.03.001.

[64] B. Qu, C.S. Bonifacio, H. Majidi, K. van Benthem, Stabilization of metal(II)oxides on the nanoscale, Mater Res Lett 8 (2020) 41–47. https://doi.org/10.1080/21663831.2019.1684395.

[65] M. Testa-Anta, M.A. Ramos-Docampo, M. Comesaña-Hermo, B. Rivas-Murias, V. Salgueiriño, Raman spectroscopy to unravel the magnetic properties of iron oxide nanocrystals for bio-related applications, Nanoscale Adv 1 (2019) 2086–2103. https://doi.org/10.1039/C9NA00064J.

[66] A.L. Drummond, N.C. Feitoza, G.C. Duarte, M.J.A. Sales, L.P. Silva, J.A. Chaker, A.F. Bakuzis, M.H. Sousa, Reducing Size-Dispersion in One-Pot Aqueous Synthesis of Maghemite Nanoparticles, J Nanosci Nanotechnol 12 (2012) 8061–8066. https://doi.org/10.1166/jnn.2012.6614.

[67] O.F.S. Khasawneh, P. Palaniandy, M. Ahmadipour, H. Mohammadi, M.R. Bin Hamdan, Removal of acetaminophen using Fe_2O_3-TiO_2 nanocomposites by photocatalysis under simulated solar irradiation: Optimization study, J Environ Chem Eng 9 (2021) 104921. https://doi.org/10.1016/j.jece.2020.104921.